OPTIMISATION OF DOUBLE DIAPHRAGM FORMING PROCESS THROUGH LOCAL ADJUSTMENT OF IN-PLANE CONSTRAINT

S. Chen, O.P.L. McGregor, L.T. Harper, A. Endruweit and N.A. Warrior

Composites Research Group, Faculty of Engineering, University of Nottingham, UK, NG7 2RD,
Shuai.Chen@nottingham.ac.uk

Keywords: Fabrics/textiles, Finite element analysis (FEA), Forming, Preform, Optimisation

ABSTRACT

In double diaphragm preforming (DDF) of non-crimp reinforcement fabrics, rigid blocks, called "risers", were introduced for adjustment of local in-plane constraints to improve fabric forming. Optimisation of the riser arrangement to minimise defect formation was implemented through riser position optimisation and riser height optimisation. A simplified finite element (FE) model was developed to simulate the DDF process for the optimisation employing a genetic algorithm (GA). The fabric behaviour was described by a non-orthogonal constitutive relation. The contribution of the diaphragms was embedded within the fabric model in regions where the diaphragm was in direct contact with the preform; in all other areas, a series of 1D spring elements were used to represent the stiffness of the diaphragm, which were connected to the edge of the fabric plies and to a rigid outer frame. Then, the optimised riser positions were adopted, and simulations were run using a detailed FE model to determine the optimal riser height. Simulations indicate that there is limited space to improve the formability by the introduction of risers in DDF. The development of this optimisation approach facilitates the discovery of the maximum capability of placing risers for defect reduction in this process.

1 INTRODUCTION

In double diaphragm forming (DDF), material plies are sandwiched between two deformable diaphragms, which are deep-drawn over a rigid tool by applying a pressure gradient normal to the surface [1, 2]. Lower capital investment is required compared to matched-tool press forming, which makes it attractive for preforming in higher volume automotive applications.

Multi-axial in-plane tension is applied to the plies through friction on the diaphragm surfaces, which can be controlled by adjusting the vacuum pressure between the diaphragms to avoid fibre wrinkling and buckling and control in-plane shear. The vacuum pressure applied between the diaphragms has a similar effect as the pressure applied through the blank holder in matched tool forming, but the compliance of the diaphragms means that the formation of defects in the fibre architecture is determined by different mechanisms. The fabric is constrained much less in DDF, therefore thickening can occur as it shears, and there is an increased risk of out-of-plane fabric buckling. One possible solution is to locally increase the tension in the fabric plies in regions prone to wrinkling. Use of 'risers', i.e. rigid blocks placed between the bed of the machine and the lower diaphragm, can help to locally increase the tensile strain in the diaphragms by increasing the effective surface area of the tool over which they are draped (see Figure 1). The position, shape and height of the risers can be modified to control the strain in regions where wrinkles are likely to occur in the fabric plies.

Optimisation of the riser arrangement to minimise defect formation was implemented using a two-step approach. In the first step, a simplified finite element (FE) model was developed to simulate the DDF process for forming non-crimp fabrics (NCF) using Abaqus/Explicit. The methodology from recent publications [2, 3] was used to model the fabric, which is described by a non-orthogonal constitutive relation. In addition, a new simplified model is presented in the current paper to describe the behaviour of the diaphragms to speed up the optimisation procedure. In this simplified model, a contribution representing the diaphragm properties is added to the fabric model in regions where the diaphragm is in direct contact with the preform. In all other areas, a series of 1D spring elements are used to represent the stiffness of the diaphragm, which are connected to the edge of the fabric plies and to a rigid outer

frame [4, 5]. Initially, the stiffness of each spring element is optimised using a genetic algorithm (GA), in order to minimise the maximum shear angle in the formed fabric. The distribution of the resulting forces around the perimeter of the fabric plies is then reproduced by introducing risers at locations where adjustment of in-plane tensile force is required. This simplification dramatically reduces CPU time, but also compromises precision. However, this step is only used to search for an approximate location for each riser, which is then further refined in the second step using the methodology previously developed by the authors [2]. The height of each riser is determined based on a detailed FE model. The simplified FE model offers an efficient way to simulate the DDF process for optimisation to indicate the effect of the distribution of in-plane constraining force on DDF. The introduction of risers in DDF provides an effective way to locally redistribute in-plane constraining forces to reduce forming defects.

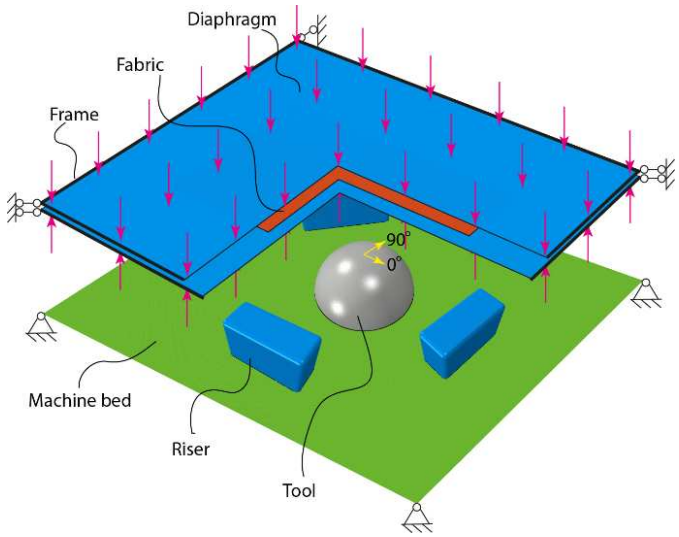

Figure 1: FE model of DDF process for riser arrangement optimisation.

2 MATERIAL DESCRIPTION

2.1 Fabric material

All preforms were made of FCIM359 biaxial carbon fibre non-crimp fabric (NCF), supplied by Hexcel, Leicester, UK. Each ply was 0.4 mm in thickness and consisted of 440 gsm of carbon fibre with a 24K tow size, in a ±45° architecture [3, 6, 7] with a pillar stitch at 0°. The effective density of the fabric was assumed to be 1200 kg/m^3. An asymmetric in-plane shear behaviour has been derived from picture frame tests [3]. The fabric behaviour was modelled using a non-orthogonal constitutive relation based on homogenisation, where the homogenised fabric modulus in each fibre direction was 138 GPa due to the assumption of no crimp in the primary yarns. The shear behaviour was expressed by the normalised shear force, F_{norm}, as a function of shear angle in radians [3]:

$$F_{norm} = F_{norm}^{yarn\ rotation} + F_{norm}^{stitch} \tag{1}$$

where the contribution of the yarn rotation was

$$F_{norm}^{yarn\ rotation} = \left(29.56\gamma_{12}^5 - 65.56\gamma_{12}^4 + 137.06\gamma_{12}^3 + 94.73\gamma_{12}^2 + 112.19\gamma_{12}\right) \text{N/m} \tag{2}$$

and the contribution of the stitch tension, considering progressive stitch failure, was described by

$$F_{norm}^{stitch} = \begin{cases} (2000\gamma_{12} - 120)\ N/m & , \quad 0.06 \leq \gamma_{12} < 0.50; \\ (-3520\gamma_{12} + 2640)\ N/m & , \quad 0.50 \leq \gamma_{12} \leq 0.75; \\ 0\ N/m & , \quad else. \end{cases} \tag{3}$$

where γ_{12} was the shear angle in radians. This material model was implemented in a user subroutine in Abaqus/Explicit. The onset of forming defects was correlated to the variation of shear angle. In positive shear, the stitch yarns are in tension and successive failure of stitch yarns starts from 28° until 43° when

the stitches fail completely. In negative shear, the stitch yarns are in compression with negligible contribution to shear modulus, and out-of-plane wrinkling of fabric ply occurs at shear angles larger than 50° mainly owing to yarn locking.

2.2 Diaphragm material

In DDF, the diaphragms were 1.56 mm in thickness and made from Supervac silicone sheet with 50 Shore A hardness, supplied by Silex Ltd, UK [1, 2]. The density of the diaphragm was 1600 kg/m^3. The hyper-elastic, non-linear stress-strain behaviour was modelled using a second order Ogden model [8], with less than 5.5% RMSE between the experimental data and the analytical approximation. The corresponding constants were obtained from the least-squares fitting as shown in Table 1, which provide a stable and accurate response of the diaphragm materials using Abaqus/Explicit.

Table 1: Material constants for Ogden hyper-elastic model used to describe the deformation of the silicone diaphragm material.

Diaphragm material	μ_1 (Pa)	α_1	μ_2 (Pa)	α_2
silicone, 1.56 mm thick	150904	3.0918	813392	0.18451

2.3 Friction between materials

The friction behaviour was tested by the authors [2] for the surface pairings in DDF, including tool-diaphragm, diaphragm-fabric and fabric-fabric contacts, according to ASTM D1894, ISO8295. In relative surface movement at constant velocity, friction coefficients were calculated from the ratio of the tangential (pulling) force and the normal force, and the average value was adopted from five repeats for each surface pairing. All of the friction behaviours in DDF were assumed to be isotropic, where the average coefficients were 0.67, 0.52 and 0.36 respectively for the pairings mentioned above.

3 METHODOLOGY

3.1 General strategy

A hemisphere with a diameter of 100 mm was formed using the DDF process. One ply of the biaxial fabric material was placed along the 0°/90° direction (see Figure 1), which was sandwiched between two diaphragms. The initial blank size for the hemisphere forming study was 300 mm × 300 mm with a thickness of 0.4 mm. A pressure differential was applied normal to the diaphragm surface, and the tensile deformation of the diaphragms around the blank provides the in-plane constraining forces to control the material forming behaviour. The placement of risers offers a promising way to adjust the distribution of in-plane constraining force by locally increase the tensile strain of the diaphragms. The riser arrangement was determined to minimise defect formation using a two-step approach: (a) Step I: Optimisation of riser position, (b) Step II: Optimisation of riser height. The optimisation in Step I was used to find sensible locations/directions to place risers, which was followed by a detailed design evaluation to finalise the geometry of each riser.

3.2 Step I: Optimisation of riser position

The major purpose of Step I was to search for an appropriate arrangement of riser locations. Although mass scaling reduced computational cost for the explicit forming simulations using an automatic scaling scheme in Abaqus/Explicit for the quasi-static DDF process, each simulation still required hours to complete [2]. This is impractical for implementing an optimisation routine, and therefore a simplified model of the DDF process is required.

The high cost of FE simulation was primarily related to the nonlinear behaviour of diaphragm material and the complex contact condition in DDF. Since the normal pressure applied to the diaphragms was high (approximately 1 bar) and the diaphragm-fabric friction coefficient was also large (0.52), the maximum available friction force could be large enough to prevent the relative displacement at this interface. Thus, in the simplified model (see Figure 2(a)), the contribution of the diaphragms was added to the fabric model in regions where the diaphragm is in direct contact with the preform. This decreased

the CPU time due to the reduction of the contact area size. In all other areas, 1D spring elements were employed to constrain the blank, which were connected to the edge of the fabric plies and to a rigid outer frame. The constraining forces from the springs could approximately replicate the in-plane constraints obtained from the diaphragms. Referring to the DDF process, obtaining larger in-plane constraining force required larger tensile strain of diaphragm. The original optimal spring force distribution could be used to determine the corresponding positions of risers. In order to generate different in-plane constraining forces, the stiffness of each spring is an optimisation variable. As shown in Figure 2(b), the required in-plane constraining force distribution from the deformation of the diaphragm was equivalently optimised by changing the local spring stiffness. The optimisation results from Step I were employed to find the positions requiring additional constraining force. Subsequently, risers were introduced at the determined places to implement the local adjustment of the constraining force in Step II by changing the riser height. Although the simplification might reduce the precision of the simulation, it was only expected to provide a start point for the next step to carry further refinement.

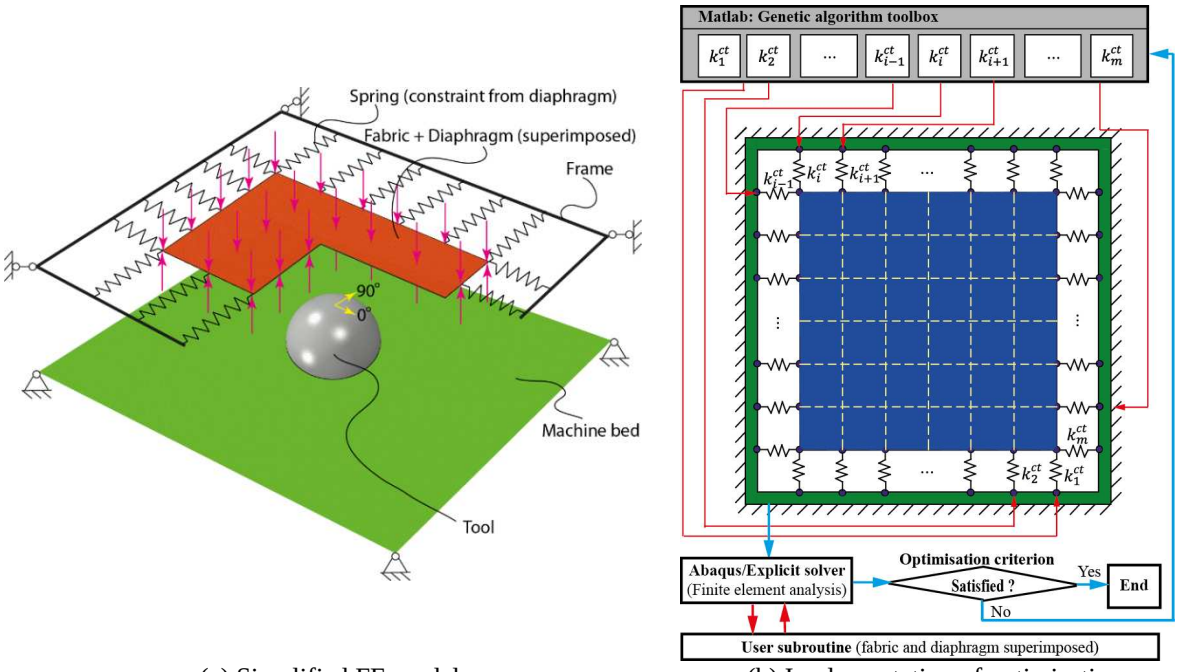

(a) Simplified FE model (b) Implementation of optimisation

Figure 2: Step I: optimisation of riser position.

In-plane constraints in the form of springs were applied to the nodes along the edge of the fabric at a 10 mm spacing. The optimisation was performed using a GA to determine optimum stiffness values for each spring from a user-defined range. The riser position optimisation was implemented using Matlab (see Figure 2(b)). For each loop or "generation" in the GA, a group of spring stiffness arrangements called "individuals" were generated, and Abaqus/Explicit input files were produced. The shear angle distribution in the deformed blank for each individual was determined from Abaqus/Explicit analyses and then returned to Matlab. The corresponding fitness value was determined from this data to check for convergence. This loop was repeated until the optimum was achieved.

For simplification, only linear behaviour was considered, which could be parameterised as

$$F_i^{ct} = k_i^{ct} d_i^{ct} \quad (i = 1,2,\dots,m) \tag{4}$$

where m is the number of springs, k_i^{ct} is the stiffness of the ith spring, d_i^{ct} is the extension of the ith spring, and F_i^{ct} is the corresponding constraining force. Consequently, the optimisation variables were converted into a stiffness $k_i^{ct}(i = 1,2,\dots,m)$.

The optimisation problem in Step I was expressed as

$$\text{minimise } f\{k_1^{ct}, k_2^{ct}, \dots, k_m^{ct}; \gamma_{12}(x,y,z)\}$$
$$\text{subject to } \begin{cases} k_i^{ct} \in \left[\left(k_i^{ct}\right)^{low}, \left(k_i^{ct}\right)^{upp}\right] \quad (i = 1,2,\dots,m) \\ \gamma_{12}(x,y,z) \in [0°, 90°] \\ (x,y,z) \in \Omega_M \end{cases} \tag{5}$$

where $f\{.\}$ is the GA fitness function to describe the selection criterion of the spring stiffness, $[(k_i^{ct})^{low}, (k_i^{ct})^{upp}]$ is the applicable stiffness range of each spring.

The fitness function was used to assess how well each individual constraining arrangement was adapted to the assessment criteria. Its value reflects the relative distance from the optimum solution, where a smaller value is preferred. A maximum value criterion (MAXVC) was adopted here due to faster convergence compared with the Weibull distribution quantile criterion (WBLQC) previously used [9], whilst maintaining acceptable accuracy. The objective is therefore to keep all local shear angles below the locking angle, by minimising the maximum shear angle. The maximum can be derived from the finite element approximation for $\gamma_{12}(x,y,z)$. Thus,

$$f_{MAXVC}\{k_1^{ct}, k_2^{ct}, \dots, k_m^{ct}; \gamma_{12}(x,y,z)\} = \max_{(x,y,z)\in\Omega_M}\{|\gamma_{12}(x,y,z)|\} \approx \max_{i=1,2,\dots,N}\{|\gamma_i|\} \tag{6}$$

where $f_{MAXVC}\{.\}$ denotes the fitness function using MAXVC, which aims to minimise the maximum shear angle; Ω_M is the spatial material region; $\gamma_{12}(x,y,z)$ is the continuous shear angle distribution in the material region, Ω_M; N is the total number of integration points; $|.|$ is the absolute value of the variable; γ_i is the value of the shear angle at the ith material point, (x_i, y_i, z_i). Since the arrangement of the spring stiffness influenced the shear angle distribution, the value of f_{MAXVC} was used for quantitative assessment of the fitness.

Once the stiffness of an arbitrary spring is larger than $[(k_i^{ct})^{low} + (k_i^{ct})^{upp}]/2$, a riser is required in the corresponding spring direction. The riser shape is limited to a cuboid in the current work, where the faces are parallel to the square base of the hemisphere tool. Each selected spring represents a riser in the length of 10 mm, which is equal to the spacing of springs. Neighbouring risers needed to be combined together to form consolidated risers. If the distance between two adjacent risers was smaller than a threshold value, they were considered to be part of the same riser. A minimum riser length was also specified, and any isolated risers were discarded. These compromises were essential for successful practical implementation, but their negative impact could be alleviated to some extent by optimising the riser height in Step II. Here, these practical considerations were implemented manually, which was facilitated by the two-stage optimisation approach. Whilst it would be feasible to include them in the optimisation code as additional constraints or regularisation terms, as previously discussed by Skordos et al. [10], this would increase the number of variables in the objective function. This would largely reduce the efficiency in automatically creating FE models, and the number of geometry variables may change during the optimisation, significantly increasing complexity. A potential solution would be to define a large enough number of variables and reserve sufficient memory, but this would be inefficient, causing computational resources to become redundant. Step I was only intended to identify sensible positions to place risers and further refinement could be achieved in Step II.

3.3 Step II: Optimisation of riser height

Since the simplified FE model was used to efficiently locate positions to place risers at the expense of reducing the precision of simulations, a detailed FE model (see Figure 1) previously developed by the authors [2] needs to be employed to finalise the optimal height of each riser in Step II. Each fabric ply was modelled in Abaqus/Explicit using 5 mm × 5 mm square membrane elements (M3D4R), which was found to be suitable in a mesh sensitivity study presented elsewhere [3]. The diaphragms were modelled using 5 mm × 5 mm S4 shell elements, which were constrained in the x-y plane around the perimeter to replicate the constraints on the diaphragm forming rig. The effective density of the fabric was $1200\ kg/m^3$, while the density of the diaphragm was $1600\ kg/m^3$. Risers were modelled as cuboid blocks placed between the bed of the machine and the lower diaphragm at the positions determined from

Step I. All parts of the tooling (tool, machine bed and risers) were modelled as rigid bodies. A penalty contact algorithm was used to define the behaviour at the interfaces. A Coulomb friction model was adopted for tool-diaphragm, diaphragm-fabric and fabric-fabric contacts. Average coefficients of friction used in the simulations were 0.67, 0.52 and 0.36, respectively, where anisotropy related to the stitching pattern in the NCF was ignored.

Pressure was applied to the upper surface of the top diaphragm and the lower surface of the bottom diaphragm, as shown in Figure 3. From time A to time B, both pressures were equal in magnitude but opposite in direction to simulate the clamping force on the fabric plies generated by the vacuum between the diaphragms. Displacement boundary conditions were then applied to the edge nodes of the diaphragms to simulate the frame holding the diaphragms being lowered to make contact with the bed of the machine. Subsequently, a pressure differential was created between the two diaphragm surfaces to simulate the vacuum being applied between the lower diaphragm and the tool. The pressure applied to the bottom diaphragm was reduced (time B to time C), drawing the diaphragm arrangement into contact with the surface of the tool. Gravity was neglected in the FE model.

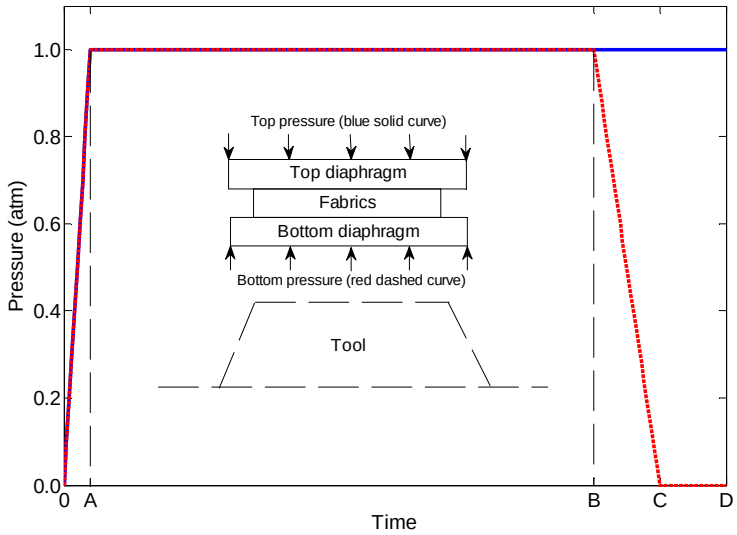

Figure 3: Definition of pressure applied to the diaphragms in the FE model.

In Step II, simulations were run to determine the effect of riser height on the fabric forming behaviour, where only discrete heights of 0 mm (i.e. no risers) 10 mm, 20 mm, 30 mm, 40 mm, 50 mm were considered. Although each individual forming simulation took about 1 hour using an Intel® Core™ i7-3820 CPU at 3.60 GHz, the process of riser height optimisation was finished in 6 hours. The evolution of the maximum shear angle using different heights of risers was plotted to seek for an optimal solution in order to reduce the defects under both positive and negative shear due to the anisotropic behaviour of the NCF material FCIM359.

4 RESULTS AND DISCUSSION

4.1 Riser position optimisation from Step I

Applying springs to the edges of the blanks at a spacing of 10 mm resulted in 31 constraining positions per each edge (i.e. 31 variables per each edge and in total 124 variables). Due to the symmetry of the blank with respect to its two diagonals, the number of independent variables was reduced to 31.

The stability of a GA in delivering an optimum solution depends on the diversity of the population [4, 5]. This is determined by the population size, the initial population and probabilities for crossover and mutation. The population size was chosen to be greater than the number of optimisation variables, using 100 for Step I (in total 31 variables). The initial population was determined randomly to ensure sufficient diversity. The crossover probability (i.e. the proportion of each population where genes from individuals in the previous generation were recombined) was 0.8, a compromise between evolution rate and solution

accuracy. The mutation probability enabled a small random variation in the individuals of each generation to create new genes, ensuring genetic diversity and enhancing the probability for an improved fitness score. Its value was determined adaptively for this study, based on the fitness scores from the previous generation.

It is important to ensure that the initial population is distributed across the entire solution space to avoid restricting the range for the optimum value. The distance between individuals in the solution space is therefore measured to quantify the diversity of the population. The stiffness of each spring was normalised by dividing the initial stiffness of the corresponding representative diaphragm strip (k_i^{rep}), calculated according to [11], where $[(k_i^{ct})^{low}, (k_i^{ct})^{upp}] = [k_i^{rep}, 5k_i^{rep}]$ was used as an optimisation constraint. For 31 variables in Step I, the normalised average distance between individuals must be less than the maximum value of 22.3 (i.e. $\sqrt{31 \times (5-1)^2}$). Furthermore, this average distance should progressively decrease for subsequent generations, indicating a reduction in search space and convergence towards the global optimum. The diversity of the population for each generation in Step I was checked by evaluating the average distance between individuals, shown in Figure 4(a). For the first five generations the value is approximately 13, indicating that the initial population covers approximately 70 % (13/22.3) of the solution space. The average distance reduces by about 1.5 % (0.33/22.3) for each generation until convergence, indicating that evolution is progressive, allowing sufficient opportunity for elite genes, i.e. genes related to low fitness scores in terms of maximum shear angles, to survive during offspring creation.

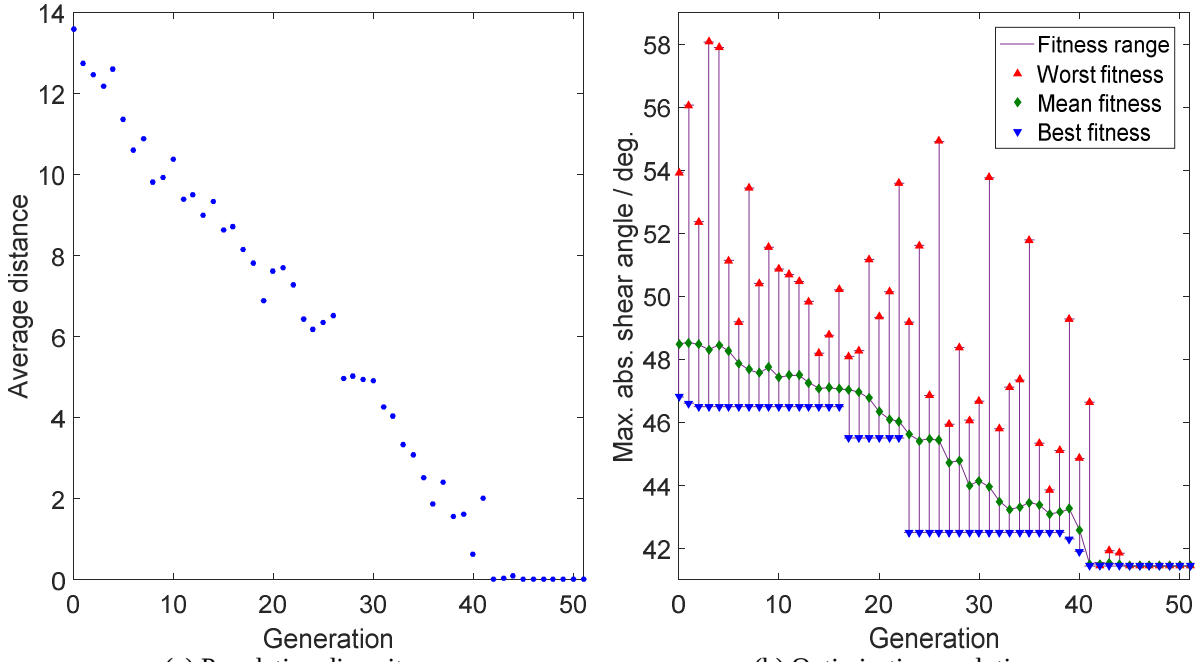

(a) Population diversity (b) Optimisation evolution

Figure 4: GA stability and convergence analyses for riser position optimisation in Step I.

Figure 4(b) shows the evolution of the fitness scores for Step I. The magnitude of the adaptive Fitness Range is similar for each generation until the Best Fitness converges, implying that a wide search range was adopted throughout. The range of the fitness score varies due to adaptive mutation. The optimum solution (i.e. convergence of the Best Fitness) is achieved during generation 41. Perturbations induced by further mutations during the next 4 generations (indicated by a non-zero fitness range) appear to have no influence on the optimum solution. Furthermore, the mutation probability reduces to zero following generation 45, after the optimum solution was determined. Therefore, Figure 4 confirms that the present diversity prevents local optimum solutions, random selection and instability.

As shown in Figure 5, a group of sensible positions to place risers were identified from Step I. Springs represented by thin lines indicate that an additional in-plane constraint is not required in that direction,

where the stiffness of the corresponding representative diaphragm strip (k_i^{rep}) is applied. A spring represented by a thick line indicates that a riser is required, where the spring stiffness was larger than $[(k_i^{ct})^{low} + (k_i^{ct})^{upp}]/2$, i.e. $(k_i^{rep} + 5k_i^{rep})/2 = 3k_i^{rep}$. The maximum shear angle in the positive shear region decreases by 9.4°, from 48.3° for the reference case with no risers (Figure 5(a)) to 38.9° when risers are placed at the optimised positions to locally adjust the constraining forces (Figure 5(b)). In the negative shear region, a significant reduction in maximum shear angle (10.3°) is also achieved using the optimised riser arrangement. Consequently, Step I is able to successfully reduce the risk of generating forming defects, especially unacceptable out-of-plane wrinkling induced by over-shearing.

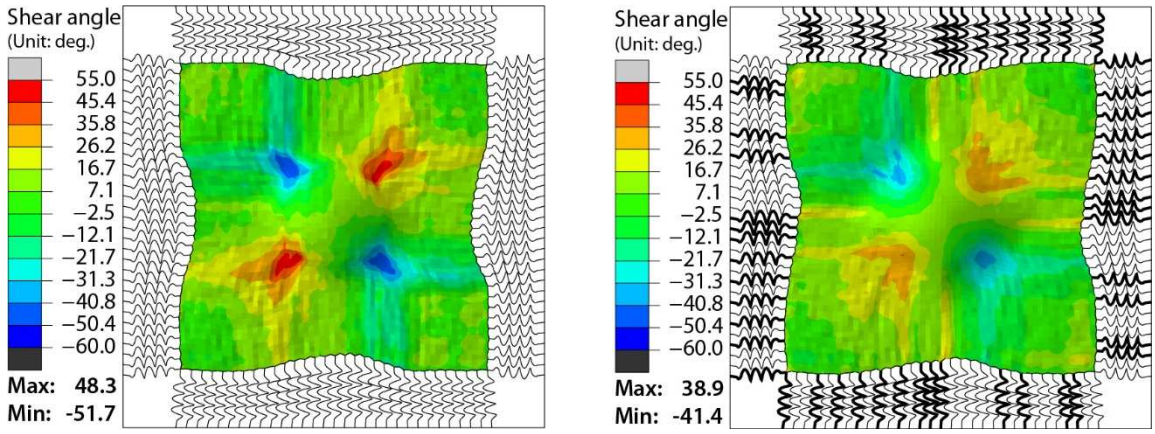

(a) Reference: no risers (b) Optimum

Figure 5: Shear angle and deformation configuration of 0°/90° preforms from DDF with optimised riser arrangement against reference case with no risers using a simplified FE model. Springs represented by thick lines indicate that a riser is required along the corresponding direction, while springs represented by thin lines indicate that no riser is required.

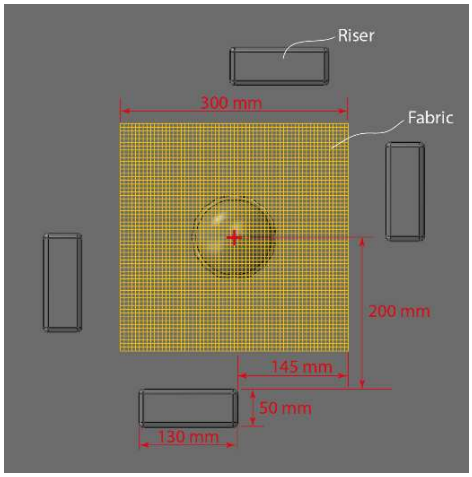

Figure 6: Optimal riser arrangement after regulating from Step I for 0°/90° preforms by DDF.

However, practical implementation of the optimal riser arrangement directly according to Figure 5(b) is infeasible, since too many individual risers are required to obtain the equivalent constraining condition. Therefore, it is necessary to compromise and combine neighbouring bold springs and eliminate isolated ones. The minimum threshold distance between bold springs was chosen to be 30 mm (equivalent to the width of 6 finite elements or 3 times the spring spacing), and the minimum clamp length was assumed to be 50 mm. Consequently, only one riser was required along each edge to maintain the optimal formability as shown in Figure 6. Each riser was 130 mm × 50 mm in the x-y plane, with 6 mm fillets around the edges, where the long edge was parallel to the corresponding undeformed blank. A distance of 200 mm was maintained from the long edge of riser to the centre of the hemisphere. These four risers were placed symmetrically with respect to the two diagonals of the undeformed square blank. The optimal height of each riser was determined from Step II.

4.2 Riser height optimisation from Step II

Risers were placed at the specified locations according to Figure 6. Simulations were run using risers of incrementally increasing height; 0 mm (i.e. no risers), 10 mm, 20 mm, 30 mm, 40 mm, 50 mm respectively. The shear angle distributions were obtained from numerical simulations using the detailed FE model as shown in Figure 7.

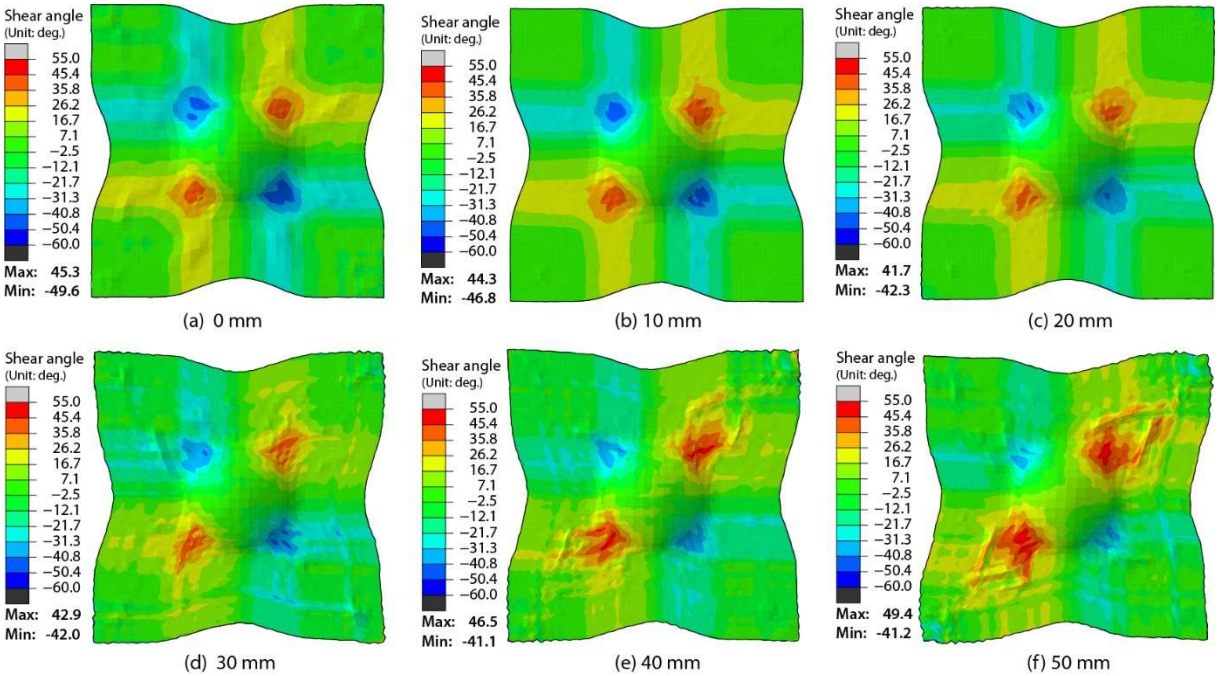

Figure 7: Shear angle and deformation configuration of 0°/90° preforms from DDF by placing risers in different heights at the optimised positions.

The shear angle distribution from the detailed FE model (Figure 7(a)) is smoother than the simplified model presented in Figure 5(a), when no risers are present. However, the prediction for the maximum shear angle and overall material deformation are very similar. There is only a 6.6 % error (48.3° compared to 45.3°) in the prediction of maximum shear angle under positive shear, and just 4.2 % (51.7° compared to 49.6°) in the negative shear region when using the simplified model.

The evolution of the maximum shear angle using different riser heights was plotted to determine an optimum solution in order to reduce the number of defects under both positive and negative shear, as shown in Figure 8. It shows that the maximum shear angle in the negative shear region decreases with increasing riser height and reaches a plateau at about 40 mm. while the one in positive shear goes through a minimum at around 20 mm to 25 mm. The two curves in Figure 8 intersect at about 26.5 mm. Although lower shear angles under both positive and negative shear are preferred to reduce the possibility of generating forming defects, the out-of-plane wrinkling defect occurs at a lower shear angle (about 43°) in positive shear than the one (around 50°) in negative shear due to the anisotropic material behaviour of FCIM359 NCF. Therefore, the optimal riser height should be chosen from the range of 20 mm to 25 mm closest to 26.5 mm to prevent the occurrence of defects in positive shear regions, which is finalised to be 25 mm.

Simulations indicate that there is limited space to improve the formability by introducing risers alone in DDF forming. Using the optimised scenario for riser arrangement, the maximum positive shear angle can be reduced to 41.6°, whilst the maximum negative shear angle can be reduced to 41.1° according to Figure 8. For other geometries of components, the maximum shear angle may not be able to be reduced below the threshold value of generating defects, which has to be confirmed using the proposed method. It indicates that risers may be unlikely to fully remove all defects in DDF for other applications, even though it has already reached its limit by optimisation. The development of this optimisation approach

is important to investigate the feasibility of placing risers for defect reduction and inform the necessity of simultaneously introducing other scenarios (such as trimming the blank shape and placing darts [1, 2, 12]).

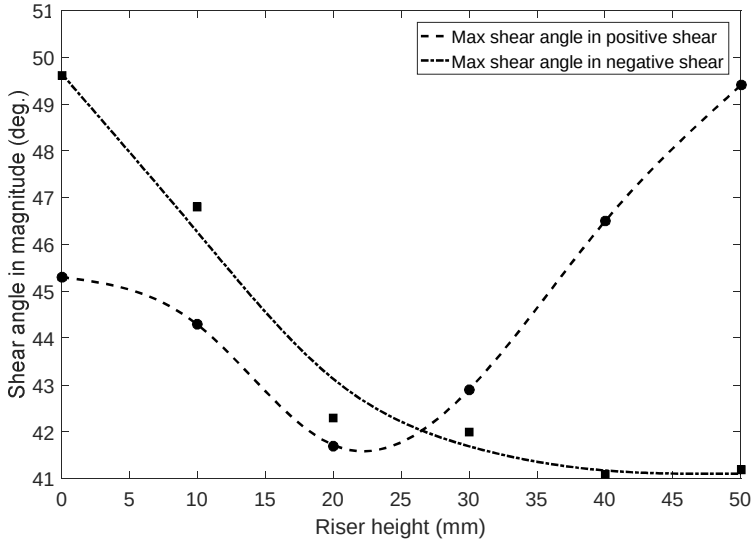

Figure 8: Evolution of maximum shear angle in both positive and negative shear for 0°/90° preforms from DDF by placing risers in different heights at the optimised positions.

5 CONCLUSIONS

A method was introduced to improve the formability of fabric material in DDF by locally adjusting the in-plane constraint using a series of rigid blocks, called “risers”. The riser arrangement was optimised to minimise defect formation.

In a first step, a FE model was developed to simulate the DDF process for forming NCF. The fabric behaviour was described by a non-orthogonal constitutive relation. A new simplified model was presented to describe the behaviour of the diaphragms to speed up the optimisation procedure. A contribution representing the diaphragm properties was added to the fabric model in regions where the diaphragm was in direct contact with the preform; in all other areas, a series of non-linear 1D spring elements were used to represent the stiffness of the diaphragm, which were connected to the edge of the fabric plies and to a rigid outer frame. Initially, the stiffness of each spring element was optimised using a GA, in order to minimise the maximum fabric shear angle. The distribution of the resulting forces around the perimeter of the fabric plies was then reproduced by introducing risers at locations where adjustment of in-plane tensile force was required. The first step is only used to search for appropriate locations for risers, and the obtained result from this step is used to initiate a second step, which further refines the geometry of the risers using a more detailed FE model.

In the second step, simulations were run to determine the effect of riser height on the fabric forming behaviour, where different heights of risers were considered. A riser height of 25 mm was found to be the optimum. Simulations indicate that there is limited space to improve the formability of the hemisphere by the introduction of risers in DDF. The development of this optimisation approach is important to investigate the maximum capability of placing risers for defect reduction.

ACKNOWLEDGEMENTS

The work presented in this paper was completed as part of the “Thermoplastic Overmoulding for Structural Composite Automotive Applications” (TOSCAA) project. The authors gratefully acknowledge the financial support of Innovate UK (Project Ref. 102663).

REFERENCES

[1] Chen, S., *Fabric forming simulation and process optimisation for composites*. 2016, University of Nottingham.
[2] Chen, S., O. McGregor, A. Endruweit, M. Elsmore, D. De Focatiis, L. Harper, and N. Warrior, *Double diaphragm forming simulation for complex composite structures.* Composites Part A: Applied Science and Manufacturing, 2017. **95**: p. 346-358.
[3] Chen, S., O. McGregor, L. Harper, A. Endruweit, and N. Warrior, *Defect formation during preforming of a bi-axial non-crimp fabric with a pillar stitch pattern.* Composites Part A: Applied Science and Manufacturing, 2016. **91**: p. 156-167.
[4] Chen, S., L. Harper, A. Endruweit, and N. Warrior, *Formability optimisation of fabric preforms by controlling material draw-in through in-plane constraints.* Composites Part A: Applied Science and Manufacturing, 2015. **76**: p. 10-19.
[5] Chen, S., L.T. Harper, A. Endruweit, and N.A. Warrior, *Optimisation of forming process for highly drapeable fabrics*, in *20th International Conference on Composite Materials*. 2015: Copenhagen Denmark.
[6] McGregor, O.P.L., S. Chen, L.T. Haper, A. Endruweit, and N.A. Warrior, *Defect characterisation and selective stitch removal in non-crimp fabrics*, in *International Conference SAMPE Europe*. 2015: Amiens.
[7] O'Sullivan, L., *Characterization and simulation of structural fabrics–Part 2: Evaluating process simulation software in a product development cycle.* Reinforced Plastics, 2015. **59**(6): p. 305-309.
[8] Ogden, R. *Large deformation isotropic elasticity-on the correlation of theory and experiment for incompressible rubberlike solids*. in *Proceedings of the Royal Society of London A: Mathematical, Physical and Engineering Sciences*. 1972. The Royal Society.
[9] Chen, S., A. Endruweit, L. Harper, and N. Warrior, *Inter-ply stitching optimisation of highly drapeable multi-ply preforms.* Composites Part A: Applied Science and Manufacturing, 2015. **71**: p. 144-156.
[10] Skordos, A., C. Monroy Aceves, and M. Sutcliffe. *Drape optimisation in woven composite manufacturing*. in *Proceedings of the 5th International Conference on Inverse Problems in Engineering*. 2005.
[11] Ehret, A.E., *On a molecular statistical basis for Ogden's model of rubber elasticity.* Journal of the Mechanics and Physics of Solids, 2015. **78**: p. 249-268.
[12] Alshahrani, H. and M. Hojjati, *Experimental and numerical investigations on formability of out-of-autoclave thermoset prepreg using a double diaphragm process.* Composites Part A: Applied Science and Manufacturing, 2017.